THE JOURNAL OF BIOLOGICAL CHEMISTRY VOL. 286, NO. 36, pp. 31480–31489, September 9, 2011

Tetrahydrofolate Recognition by the Mitochondrial Folate Transporter*[S]

Received for publication, June 14, 2011, and in revised form, July 6, 2011 Published, JBC Papers in Press, July 15, 2011, DOI 10.1074/jbc.M111.272187

Scott A. Lawrence[‡], John C. Hackett[§¶], and Richard G. Moran[‡‖1]

From the Departments of [‡]Pharmacology and Toxicology and [§]Medicinal Chemistry, [¶]Institute for Structural Biology and Drug Discovery, and [‖]Massey Cancer Center, Virginia Commonwealth University, Richmond, Virginia 23298

A mitochondrial carrier family (MCF) of transport proteins facilitates the transfer of charged small molecules across the inner mitochondrial membrane. The human genome has ~50 genes corresponding to members of this family. All MCF proteins contain three repeats of a characteristic and conserved P*X*(D/E)*XX*(K/R) motif thought to be central to the mechanism of these transporters. The mammalian mitochondrial folate transporter (MFT) is one of a few MCF members, known as the P(I/L)W subfamily, that have evolved a tryptophan residue in place of the (D/E) in the second conserved motif; the function of this substitution (Trp-142) is unclear. Molecular dynamics simulations of the MFT in its explicit membrane environment identified this tryptophan, as well as several other residues lining the transport cavity, to be involved in a series of sequential interactions that coordinated the movement of the tetrahydrofolate substrate within the transport cavity. We probed the function of these residues by mutagenesis. The mutation of every residue identified by molecular dynamics to interact with tetrahydrofolate during simulated transit into the aqueous channel severely impaired folate transport. Mutation of the subfamily-defining tryptophan residue in the MFT to match the MCF consensus at this position (W142D) was incompatible with cell survival. These studies indicate that MFT Trp-142, as well as other residues lining the transporter interior, coordinate tetrahydrofolate descent and positioning of the substrate in the transporter basin. Overall, we identified residues in the walls and at the base of the transport cavity that are involved in substrate recognition by the MFT.

Folate metabolism is essential for mammalian cell survival and consists of reaction sequences that occur in the mitochondrial and cytosolic compartments. In dividing cells, cytosolic folate metabolism uses one-carbon units for purine nucleotide and thymidylate synthesis, whereas mitochondrial folate metabolism primarily drives the supply of formate to the cytoplasm for these processes. Mitochondrial folates are also used as cofactors for mitochondrial glycine synthesis, and cells deficient in mitochondrial folate metabolism are auxotrophic for glycine despite the fact that enzymes capable of glycine synthesis are present in both compartments (1–5). An example of such glycine auxotrophy is the Chinese hamster ovary (CHO)-derived glyB cell, which retains wild-type activity of all the enzymes involved in mitochondrial folate metabolism but is unable to accumulate mitochondrial folates (1–3). Previously, we used complementation of glycine auxotrophy with a retroviral cDNA library to isolate the gene defective in glyB cells; it encoded a protein that transported folates into mitochondria, the mitochondrial folate transporter (MFT)[2] (3). In glyB cells, the MFT open reading frame has a G192E missense mutation that diminishes mitochondrial folate levels by ~99% and effectively eliminates the transport of mitochondrial folates (2, 3). Transfection of cDNAs encoding MFT orthologs from human, mouse, hamster, zebrafish, and *Arabidopsis thaliana* into glyB cells restored mitochondrial folate transport and eliminated the glycine auxotrophy (2).

The MFT is a member of a larger solute carrier family known as the mitochondrial carrier family (MCF); it has been assigned the number SLC25A32. The MCF is comprised of at least 46 human (6) and ~35 yeast mitochondrial inner membrane integral proteins that are 30–35 kDa in size and import small charged compounds into the mitochondrial matrix. All MCF proteins consist of three tandem repeats of ~100 amino acids, with a conserved P*X*(D/E)*XX*(K/R) motif located immediately after the first, third, and fifth of six transmembrane domains (TMD) (7). An x-ray crystallographic structure of one MCF transporter, the bovine ADP/ATP carrier (AAC) (7), was solved at high resolution as a complex with a tight-binding inhibitor, carboxyatractyloside. The solved AAC structure revealed a funnel-shaped, aqueous transport cavity formed by six α-helical transmembrane spans. Located about two-thirds of the way down into the AAC transport cavity, the odd-numbered transmembrane spans had angular kinks at the positions of the conserved motif proline residues. An apparent cavity floor was formed by three symmetrical ionic bonds between the (D/E) and (K/R) residues of adjacent conserved motifs (7); these interactions are thought to be central to the transport mechanism of all MCF proteins. It has been proposed that the charged transport substrate disrupts the symmetrical salt bridge interactions between these residues and initiates a momentary widening of the channel for substrate passage (7–10).

Despite this proposed common mechanism of opening, MCF transporters are able to discriminate between and transport

* This work was supported, in whole or in part, by National Institutes of Health Grant R01-CA104279 (to R. G. M.).

[S] The on-line version of this article (available at http://www.jbc.org) contains supplemental Figs. 1–4.

[1] To whom correspondence should be addressed: 401 College St., P. O. Box 980035, Richmond, VA 23298. Tel.: 804-828-5783; E-mail: rmoran@vcu.edu.

[2] The abbreviations used are: MFT, mitochondrial folate transporter; MCF, mitochondrial carrier family; AAC, ADP/ATP carrier; MD, molecular dynamics; TMD, transmembrane domain; 5f-thf, (6*S*)-5-formyl-tetrahydrofolate; POPC, palmitoyloleoylphosphatidylcholine; NPT, constant temperature and pressure.

different molecules with high specificity. Based on computational docking into homology models of nine MCF proteins and bioinformatics analysis of ~40 MCF primary sequences, Robinson and Kunji (9) proposed that there were three substrate-binding sites common to all MCF proteins where amino acid differences explained the substrate specificities of individual transporters. There is a clear need to study individual MCF proteins to support and expand upon the insights offered by the work of Robinson and Kunji. Thus, Ma *et al.* (11) used a combination of site-specific mutagenesis with homology modeling and computational docking and identified several residues that constituted a second substrate-binding site within the citrate transport cavity that was not identified by Robinson and Kunji. In this study, we have sought to identify specific residues in the MFT that interact with the tetrahydrofolate ligand and potentially play a role in the substrate selectivity of this transporter.

The MFT differs from most other MCF proteins in that it is one of only five MCF proteins, known as the P(I/L)W subfamily, that contain a tryptophan residue (hamster MFT Trp-142) substituted in place of the (D/E) residue found in all other MCF proteins in the conserved motif on TMD 3. This tryptophan substitution is interesting because it would disrupt one of the three proposed ionic bonds formed between conserved motifs and possibly alter the proposed common MCF transport mechanism in P(I/L)W subfamily members. We previously proposed that a π-cation interaction (12) in the MFT substituted for the putative electrostatic interaction present in all other MCF transporters based on the observation that the basic residue in the conserved motif on TMD 5 in the hamster MFT, Arg-249, was required for MFT function (13). Thus, although three ionic interactions would not be present at the base of P(I/L)W transporters, it is likely that three interactions form between the P(I/L)W conserved motifs and that a very similar mechanism of channel opening was operative in these transporters. Nonetheless, this tryptophan substitution raises questions regarding the potential differences between P(I/L)W proteins and other MCF members with respect to substrate recognition and the transport process.

In this study, we used a complementary approach including molecular dynamics simulations, site-specific mutagenesis, and transport kinetic studies to investigate the residues required for MFT function. The results of these studies indicate that substrate discrimination in the MFT is an ordered process in which the substrate is involved in sequential interactions with hydrophobic and electrostatic residues that line the transport cavity at increasing depths down the channel. The substrate must be efficiently shuttled from one binding partner to the next, and interactions occurring higher in the channel are prerequisites for those that occur deeper within the transport cavity. In each case, the absence of a predicted contact residue significantly impaired transport. We postulate that the interactions with residues that guide the transport substrate down the channel determine the substrate specificity of this type of transporter.

EXPERIMENTAL PROCEDURES

Generation of the Hamster MFT Homology Model—A homology model of the hamster MFT was previously created in Tripos Sybyl v7.1 (13). Transmembrane spans predicted by the PSIPRED server (14) and the conserved motifs of the MFT were aligned with those of the bovine AAC sequence (Protein Data Bank (PDB) ID: 1OKC) and modeled as structurally conserved regions (supplemental Fig. 1). This model was modified using Tripos Sybyl 8.0 ORCHESTRAR (15) to improve the fit of MFT loop regions, using the enhanced libraries of loop structures of that version. Alignment gaps or predicted loop regions in the MFT were modeled independent of the AAC structure. Following generation of the hamster MFT homology model, the model was analyzed and adjusted so that no peptide bond distances were >20% from 1.33 Å, and the ϕ and ψ angles of all residues were at least within the allowed regions of the Ramachandran plot.

Molecular Dynamics Simulation of the Mitochondrial Folate Transporter—A square 100 Å^2 palmitoyloleoylphosphatidylcholine (POPC) bilayer membrane slab was constructed using the Visual Molecular Dynamics (VMD) program (16), and an additional 30 and 20 Å of TIP3P water molecules were added to the intermembrane space and matrix sides, respectively. All molecular dynamics (MD) simulations were performed with the NAMD 2.6 suite of programs (17) and the CHARMM22 (18) force field for biomolecular simulations. The hydrated membrane was minimized for 5000 steps followed by equilibration of the aliphatic lipid tails for 500 ps at constant volume and temperature (300 K). After melting of the lipid tails, the entire membrane system was equilibrated in the constant volume and temperature ensemble for an additional 500 ps.

The propKa module of the PDB2PQR suite of programs (19–21) was used to calculate estimates of pK_a values for ionizable residues in the MFT homology model. These values as well as visual inspection of local side chain environments were subsequently used to assign their protonation states at pH 7.4. All acidic residues were deprotonated (negatively charged), whereas arginine and lysine residues were protonated (positively charged). Histidine residues were either doubly protonated (MFT 20, 41, 67, 213, 256, 305) or singly protonated at N$^{\delta}$ (MFT 195); none were singly protonated at N$^{\epsilon}$. After the appropriate adjustments in the protonation states, the MFT homology model was oriented in the center of the pre-equilibrated POPC membrane. Overlapping lipid and water molecules, as well as those within 0.8 Å, were removed from the simulation system. Nineteen chloride ions were added to neutralize the simulation cell resulting in a system containing ~100,000 atoms for molecular dynamics simulation. The complete system was minimized for 5000 steps followed by equilibration of the lipid tails for 200 ps with the coordinates of the remaining atoms in the system frozen. Melting of the lipid tails around the MFT protein was followed by an additional 1000 steps of minimization and equilibration for 200 ps at constant temperature and pressure (NPT) using the Langevin piston method (22, 23) with a target pressure of 1.01325 bar, decay period of 100 fs, and piston temperature of 300 K. The area of the membrane was maintained constant during NPT simulations. This minimization and equilibration protocol was then repeated, albeit with a harmonic restraint (5 kcal/mol/Å) applied to the protein backbone atoms. In these preparative NPT MD simulations, harmonic forces (0.1 kcal/mol/Å) were applied between select water molecule oxygen atoms and the C21 atoms of the POPC

lipids to prevent water molecules from entering the hydrophobic phase of the membrane during equilibration. Prior to production simulations, an additional 2 ns of NPT simulation was performed with these restraints applied between the water and lipid molecules to ensure equilibration and packing of the POPC membrane around the MFT protein. After completion of the preparative simulations, the MFT model was equilibrated for an additional 30 ns. This homology model was stable throughout the MD simulations without constraints, as evidenced by the root mean square deviation of the atoms in the backbone of the MFT homology model TMDs (supplemental Fig. 2).

CHARMM parameters for tetrahydrofolate (THF) were derived from dihydrofolate parameters (24). Electrostatic potential charges were derived using the CHELPG scheme (25) from a fully optimized geometry at the B3LYP/6-31G(d) level of theory (26–28) using the Gaussian 03 suite of programs (29). To simulate capture of THF by the MFT model, this ligand was merged with the trajectory snapshot corresponding to $t = 5$ ns. Overlapping water molecules as well those within 0.8 Å of THF were removed from the simulation system. To compensate for the dianionic tetrahydrofolate and maintain electrical neutrality of the simulation cell, two chloride ions were removed. Unless otherwise noted, THF-containing systems were subjected to 40 ns of molecular dynamics simulation in the NPT ensemble at 300 K.

Generation of Mutant MFT cDNA Constructs—Site-directed mutagenesis of the N-terminally *myc* epitope-tagged hamster MFT in pcDNA 3.1(−) was carried out by overlap extension PCR (30), as described previously (13). All constructs were sequenced prior to use.

Transfection of glyB Cells and Complementation Assay—CHO-derived glyB cells (1) were routinely grown in MEM-α medium supplemented with 10% fetal bovine serum (FBS). glyB cells were transfected with N-terminal *myc*-tagged hamster MFT mutant cDNAs as described previously (13) with minor modifications. Cells were plated at 1×10^5 cells/100-mm dish 48 h prior to transfection and were transfected using a calcium phosphate-based method (13, 31). Cells were fed fresh medium 24 h after transfection but were not exposed to dimethyl sulfoxide (DMSO). For the glyB complementation assay, selective medium consisting of either glycine-free MEM-α supplemented with 10% dialyzed FBS and 1 mg/ml Geneticin for double selection or glycine-containing MEM-α with 10% dialyzed FBS and 1 mg/ml Geneticin for single selection was added to the cells 48 h after transfection. Colonies formed on triplicate plates were fixed, stained, and manually counted. The data shown represent the average of 3–6 experiments.

Two methods were used to generate clonal cell lines for transport studies. In both methods, glyB cells were transfected as above, and individual colonies were isolated and mass-cultured in single selection medium. Ten clones were expanded for each mutation. The cell lines used in Fig. 4 were derived from a single clone after screening the 10 clones by immunoblotting for the *myc* epitope and selection of the clones in which MFT expression and insertion into mitochondria were most closely matched. The cell lines used in Fig. 5 were created by pooling equal numbers of cells from all 10 clones as described previously (13).

Isolation of Mitochondria—Cells were scraped from growth dishes in phosphate-buffered saline (PBS) with a commercial mixture of EDTA-free protease inhibitors (Roche Applied Science). Cells were collected by centrifugation and resuspended in 7.5 ml of homogenization solution (250 mM sucrose; 1 mM EDTA; pH 6.8) with protease inhibitors. After a 5-min incubation in homogenization solution, cells were lysed using 15 strokes in a Dounce homogenizer. Mitochondria were isolated by differential centrifugation (13).

Mitochondrial Uptake of (6S)-5-Formyl-tetrahydrofolate—Cells were detached from growth dishes using trypsin/EDTA, resuspended in MEM-α medium supplemented with 10% FBS, and placed in a 37 °C shaking incubator to allow recovery from trypsin exposure for 1 h. Cells were collected by centrifugation, resuspended in 0.25 ml of RPMI 1640 medium without folic acid or serum at 10–20 $\times$ 10^6 cells/ml, and placed in a 37 °C shaking water bath for 5 min. Uptake was initiated by the addition of an equal volume of RPMI 1640 medium without folic acid but containing 0.25 μM (6*S*)-[3′,5′, 7,9-^{3}H]5-formyl-tetrahydrofolate (Moravek Radiochemicals) at a final specific activity of 10 Ci/mmol. Uptake was stopped by the timed addition of 10 ml of ice-cold PBS. Cells were collected by centrifugation and washed twice with 10 ml of PBS, and mitochondria were isolated as described above. Radioactivity was determined by scintillation counting.

Detection of myc-MFT by Western Blotting—Mitochondria were isolated as described above and resuspended in lysis buffer (62.5 mM Tris, pH 6.8; 5% glycerol; 2% SDS; 5% 2-mercaptoethanol) with protease inhibitors. Mitochondrial protein concentrations were determined with the Bradford method against a standard of bovine serum albumin. Twenty micrograms of mitochondrial protein were resolved on a 12% SDS-PAGE gel, and the fractionated proteins were transferred to a PVDF membrane in a buffer containing 192 mM glycine and 25 mM Tris (pH 8.3). Nonspecific membrane binding was minimized by a 1-h wash with Starting Block T20 (Thermo Fisher Scientific) followed by three washes in Tris-buffered saline containing 0.05% Tween (TBS-T) for 5 min each. The membrane was incubated with rabbit anti-*myc* antibody (Sigma) in Starting Block T20 (1:1000 dilution) at 4 °C for 16 h. The membrane was then washed three times for 5 min each in 0.05% TBS-T and placed in Starting Block T20 with peroxidase-conjugated donkey anti-rabbit IgG antibody (1:15,000 dilution, Thermo Fisher Scientific) for 1 h followed by three washes for 5 min in 0.05% TBS-T. Protein-containing membranes were incubated with Super-Signal West Dura chemiluminescent substrate (Pierce) and exposed to x-ray film.

RESULTS

Simulation of the Descent of THF into the Transport Cavity of the MFT—MD simulations of the hamster MFT were performed in an explicit membrane environment. Prior to the addition of the THF substrate, the simulation system was allowed to equilibrate for 30 ns. The time-averaged electrostatic potential surface was computed using the PMEpot (32) plug-in of VMD utilizing frames from the first 5 ns of the sim-

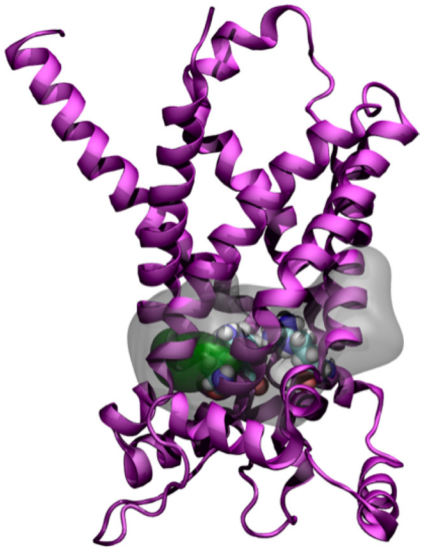

FIGURE 1. **The time-averaged electrostatic potential surface of the initial 5 ns of the apo-MFT NPT simulation was computed using the PMEpot plug-in of VMD.** The hamster MFT homology model is shown in *purple ribbon*, and residues Lys-47, Lys-145, and Arg-249 are shown in the van der Waals representation. Volumes that correspond to a +1.0 V electrostatic potential and a +1.5 V electrostatic potential are shown in *gray* and *green*, respectively.

ulation. The MFT was found to maintain a positive electrostatic potential at the base of the transport cavity with a maximum of +1.9 V as illustrated in Fig. 1. This established an electrostatic gradient that attracted the negatively charged THF molecule down into the cavity.

THF was manually oriented at several heights from the base of the transport cavity. The initial simulations oriented the tetrahydrofolate substrate with the carboxylates pointed down into the channel. When the simulation was initiated with the THF ligand ~42 Å above the transporter basin, THF diffused into the aqueous environment. In a second simulation with THF oriented ~28 Å above the base of the transporter, the carboxylate anions were captured by positively charged residues in the intermembrane space loop regions of the MFT and did not enter the transport cavity. However, orientation of the THF ligand 25 Å above the transporter basin resulted in capture of the THF ligand by the transport cavity. Two simulations were conducted with the carboxylates of the THF ligand 25 Å above the transporter basin. The first simulation was performed for 40 ns; the results of this simulation are representative of all subsequent simulations and are discussed herein. The second simulation with the "carboxylates down" was performed until the ligand nestled into the transporter basin in an identical binding mode to the aforementioned simulation. A third simulation was performed with the pteridine ring oriented 25 Å above the channel basin and the carboxylates toward the intermembrane space side and solvent water. To our surprise, the THF substrate reoriented itself during the initial stages of the simulation, enabling the carboxylates to lead the way down into the cavity and for THF to nestle into the base of the channel in a binding mode identical to that observed in simulations with the carboxylates down (supplemental Fig. 3).

THF transit to the base of the transport cavity was driven by a cascade of interactions involving multiple residues (Fig. 2). In the 40-ns simulation with the carboxylates down, the γ-carboxylate of THF initially established an ionic interaction with the ONIUM functionality of Lys-235. As the simulation evolved, Lys-235 released the γ-carboxylate of THF and reformed an ion pair with the α-carboxylate at $t = 5$ ns (Fig. 2, *A*, *D*, and *E*). As Lys-235 paired with the α-carboxylate, Tyr-300 secured the pteridine ring of THF, and both interactions were maintained until $t = 14$ ns (Fig. 2, *A* and *F*). At $t = 14$ ns, Arg-249 captured the γ-carboxylate of THF (Fig. 2, *B* and *D*), an interaction that pulled the THF molecule deeper into the transport cavity and afforded concomitant transfer of the α-carboxylate from Lys-235 to Arg-288 (Fig. 2, *B* and *E*). The interactions of the α- and γ-carboxylates of THF with MFT Arg-288 and Arg-249, respectively, were remarkably stable and represented the final configuration at $t = 40$ ns (Fig. 2, *C–E*). However, after $t = 14$ ns, the phenyl and pteridine rings of THF remained mobile within the MFT transport cavity relative to the anchored THF carboxylates. The pteridine ring of THF transiently contacted Phe-200 on MFT TMD 4 ($t = 15$ ns) (Fig. 2, *B* and *F*), which allowed the amide carbonyl of THF to move into contact with the indole nitrogen of Trp-142 and in close proximity to Gly-91 ($t = 20$ ns) (Fig. 2, *C* and *G*). Once the amide carbonyl of THF was stabilized by interaction with Trp-142, the pteridine ring of THF moved to stack with Trp-96 at $t = 25$ ns (Fig. 2, *C* and *F*). After $t = 25$ ns, the carboxylate, phenyl ring, and pteridine ring environments were unchanged for the remainder of the simulation. This THF binding mode may reflect a pretransport state of the THF-MFT complex. Overall, these simulations suggested an important role for MFT residues Gly-91, Trp-96, Trp-142, Phe-200, Lys-235, Arg-249, Arg-288, and Tyr-300; these residues were investigated by mutagenesis (below).

Because the conserved motifs are thought to play a central role in the function of all MCF transporters, the fluidity of interactions between the residues putatively holding these peptides together and establishing a transport barrier was examined in MD simulations. Homology modeling of the hamster MFT had previously predicted interactions between Asp-44 and Lys-145, Trp-142 and Arg-249, and Gln-246 and Lys-47 (13); the distances between these residues were monitored for the duration of the THF-MFT MD simulation. These pairs of residues were noticeably mobile and were spatially separated for the initial half of the simulation (Fig. 3*A*). Interestingly, these three pairs of residues migrated to within ionic bond distance only when the THF substrate was oriented immediately adjacent to them deep within the MFT transport cavity and appeared to be held in place by the proximity of the transport substrate. The formation of a hydrogen bond between the amide carbonyl of THF and the indole nitrogen of Trp-142 correlated in time (20 ns) with the tightening of the canonical transport barrier (Figs. 2*G* and 3*A*). We also performed simulations on the MFT homology model in the absence of substrate (apo-MFT) for 30 ns. In the absence of the effect of THF on the mobility of these peptides, the bonding between the conserved motif residues was not stable and did not appear to be intact at the end of this simulation (Fig. 3*B*).

Mitochondrial Folate Uptake in Cells Stably Transfected to Express MFT Gly-91, Trp-142, and Arg-249 Mutant Proteins—MD simulations suggested that the residues proposed to form a π-cation interaction, Trp-142 and Arg-249, were involved in

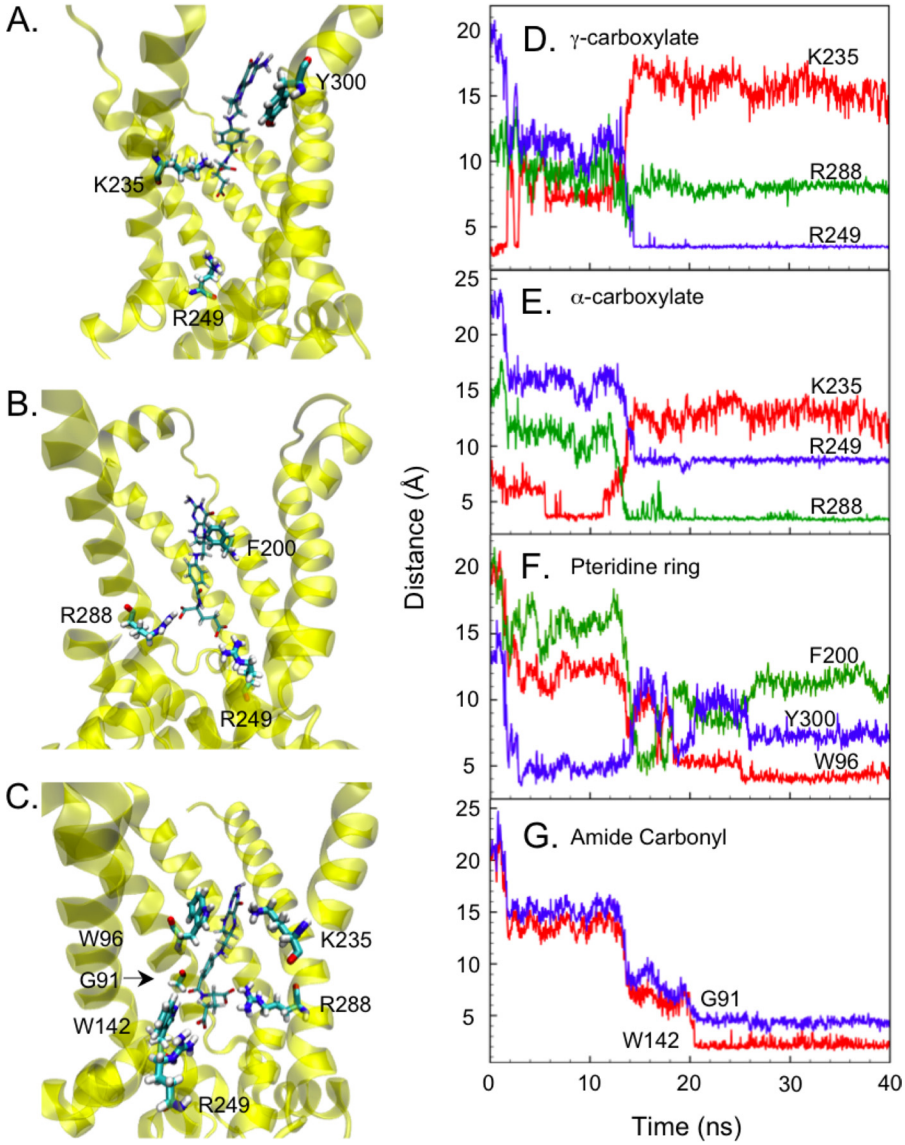

FIGURE 2. **Molecular dynamics simulation of tetrahydrofolate capture by the MFT.** *A–C*, orientation of the THF substrate within the hamster MFT homology model transport cavity at 5 (*A*), 9 (*B*), and 40 ns (*C*) during the THF-MFT MD simulation. *D–G*, time evolution of distances (Å) between the indicated hamster MFT residues and the γ-carboxylate of THF (*D*), the α-carboxylate of THF (*E*), the pteridine ring of THF (*F*), and the amide carbonyl of THF (*G*) was measured throughout the duration of the THF-MFT MD simulation. Distances were calculated between the coordinates of the respective centers of mass for the amino acid side chains as well as THF functional groups: α- and γ-carboxylate groups of THF (Cδ, O1δ, O_2δ); Lys-235 (NεH_3); Gly-91 (backbone carbonyl oxygen); Trp-96 and Trp-142 (indole ring atoms); Phe-200 (phenyl unit); Arg-249, Arg-288 (guanidinium); and Tyr-300 (phenol unit).

substrate binding and that Gly-91 was in close proximity to the phenyl ring of the THF substrate at the base of the transport cavity. Interestingly, other MCF transporters have been shown to require a basic residue for transport function at the position homologous to hamster MFT Gly-91 (11, 33, 34), and we questioned whether the small size and uncharged nature of this residue were essential for function of the MFT. We also used mutagenesis to query the presence of and functional requirement for a proposed π-cation interaction between Trp-142 and Arg-249 as well as to probe position 142 for the requirement of charge, size, and aromatic character.

An assay was designed to directly measure uptake of folates into mitochondria in intact glyB cells that had been stably transfected with cDNAs encoding mutant MFT proteins to assess the effects of various mutations on MFT transport function. Exposure of intact cells to 0.25 μM extracellular [^{3}H]5-f-thf resulted in the time-dependent accumulation of labeled folates in mitochondria from MFT wild-type CHO cells but little detectable uptake into mitochondria from the CHO-derived glyB cells (Fig. 4*A*). Cloned glyB derivative cell lines were created by stable transfection with mutated hamster MFT cDNAs bearing an N-terminal *myc* tag. The N-terminal *myc* tag had been previously shown to have a minor impact on MFT function (13), but it allowed us to follow the intracellular trafficking of the encoded mutant MFT proteins and to select transfectant clones for equivalent levels of MFT expression. All mutant MFT proteins were found in the mitochondrial protein fraction, an indication that the transfected MFT proteins were targeting correctly to mitochondria (Fig. 4*B*). The transport of folates into mitochondria of cells expressing mutant MFT species was estimated by incubating cells with [^{3}H]5-formyl-tetrahydrofolate for 4 min and determining the folate content of

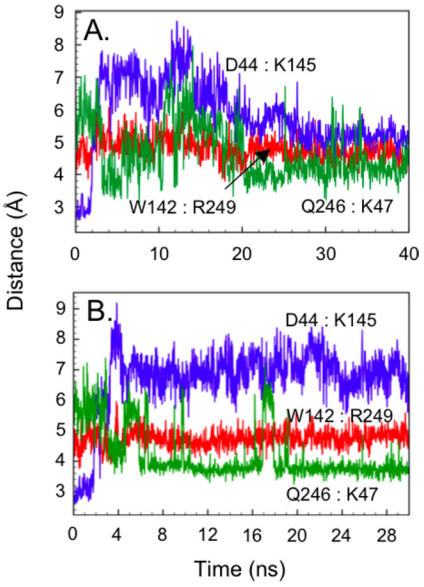

FIGURE 3. **Conserved motif interactions during THF-MFT and apo-MFT MD simulations.** *A* and *B*, time evolution of distances between MFT conserved motif residues predicted to interact, on the basis on the AAC crystal structure and homology modeling, throughout the duration of the THF-MFT MD simulation (*A*) and the apo-MFT MD simulation (*B*). The MFT conserved motif residues predicted to interact are Asp-44-Lys-145 (*blue*), Trp-142-Arg-249 (*red*), and Gln-246-Lys-47 (*green*). Distances were calculated between the coordinates of the respective centers of mass for the amino acid side chains: Asp-44 (Cδ, O1δ, O_2δ); Lys-47 and Lys-145 (NϵH_3); Trp-142 (indole ring atoms); Gln-246 (Cϵ, Oϵ, NϵH_3); and Arg-249 (guanidinium).

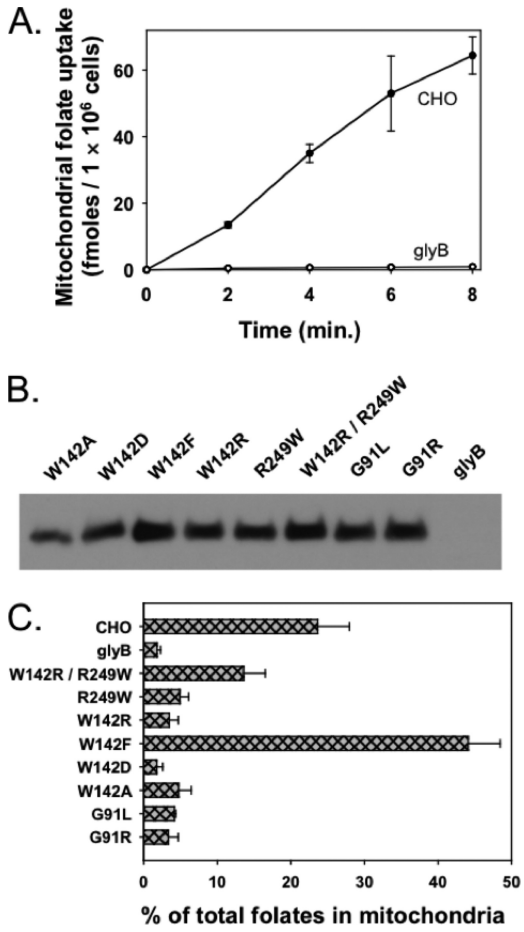

FIGURE 4. **Time-dependent uptake of mitochondrial folates in mutant MFT stable transfectants.** *A*, MFT wild-type hamster and glyB cells were incubated with 0.25 μM [^{3}H]5-f-thf for the indicated periods of time, after which mitochondria were isolated from cells and the radioactive content in mitochondria was determined. *Error bars* indicate S.D. *B*, mitochondrial protein (20 μg) from untransfected glyB cells or glyB cells stably transfected with the indicated MFT mutant cDNAs was probed for the expression of an N-terminally *myc*-tagged MFT protein by Western blotting to determine proper protein trafficking and estimate MFT expression level. *C*, cells stably transfected with cDNAs encoding the indicated MFT mutant proteins were incubated with [^{3}H]5-f-thf for 4 min, after which mitochondria were isolated and the radioactive content in mitochondria was determined. Mitochondrial folate uptake in untransfected CHO and glyB cells was included as a positive control and a negative control, respectively. *Error bars* indicate S.D.

isolated mitochondria. Most of the mutations made at positions Gly-91, Trp-142, and Arg-249 had severely depressed rates of uptake into mitochondria when compared with CHO cells (Fig. 4*C*). Change of the residue at position 142 to a basic, (W142R), neutral (W142A), or acidic (W142D) residue resulted in mitochondrial folate uptake rates that were as low as or slightly higher than that seen in glyB cells. It is notable that the residue at position 142 present in almost all MCF members, Asp, did not support mitochondrial folate transport *in vivo* despite the fact that it would have been predicted to form an ionic bond with Arg-249. The mutation of Trp-142 to a Phe, which would be compatible with retention of a π-cation bond with Arg-249, allowed efficient uptake of folates into mitochondria, and the reciprocal double mutation W142R/R249W, which would also allow formation of a π-cation interaction between these two positions, allowed >50% mitochondrial folate uptake rates. Replacement of Gly-91 with either an Arg residue, as is most frequently seen in mitochondrial nucleotide transporters such as the AAC, or even the neutral but moderately bulky G91L mutation, was incompatible with efficient transport function. We concluded that these functional studies supported the concept that a π-cation bond between Trp-142 and Arg-249 was intrinsic to the transport mechanism in the MFT and that the positioning of the THF substrate in coordination with Trp-142 and Arg-249 required a small and uncharged residue side chain at position 91.

Examining the Role of Trp-96, Phe-200, Lys-235, Arg-288, and Tyr-300 in MFT Function—The MD simulations described above predicted several residues that line the MFT aqueous cavity to interact with the transport substrate during the entry into and transit down the transport cavity. Thus, Trp-96, Phe-200, and Tyr-300 were all predicted to contact the aromatic groups of THF, whereas Lys-235 and Arg-288 were predicted to form ionic bonds with the carboxylate groups of THF. Each of these residues was a putative substrate contact point that served to relay the THF substrate to the base of the transport cavity; the transient interactions established between the substrate and these channel-lining residues appeared to be successive tests of the molecular structure, shape, and flexibility required for acceptance as a transport ligand. We used alanine-scanning mutagenesis to test the validity of the roles predicted for these residues by MD simulation. As also seen in the mutants studied in Fig. 4, the *myc*-tagged MFT proteins in this series of mutations correctly trafficked to mitochondria and were present in near equivalent levels (Fig. 5*A*). The uptake of [^{3}H]5-f-thf into mitochondria in stably transfected cell lines expressing these mutant MFT proteins was determined as before. For each of the amino acids predicted to play a signifi-

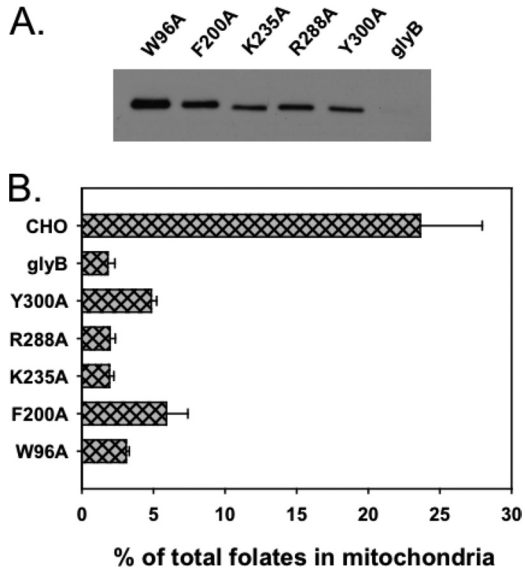

FIGURE 5. **Alanine-scanning mutagenesis of other MFT residues identified by MD simulations.** *A*, mitochondrial protein (20 μg) from untransfected glyB cells or glyB cells stably transfected with the indicated MFT mutant cDNAs was probed for the expression of an N-terminally *myc*-tagged MFT protein by Western blotting to determine proper protein trafficking and estimate MFT expression level. *B*, cells stably transfected with cDNAs encoding the indicated MFT mutant proteins were incubated with [^{3}H]5-f-thf for 4 min, after which mitochondria were isolated and the radioactive content in mitochondria was determined. Mitochondrial folate uptake in untransfected CHO and glyB cells was included as a positive control and a negative control, respectively. *Error bars* indicate S.E.

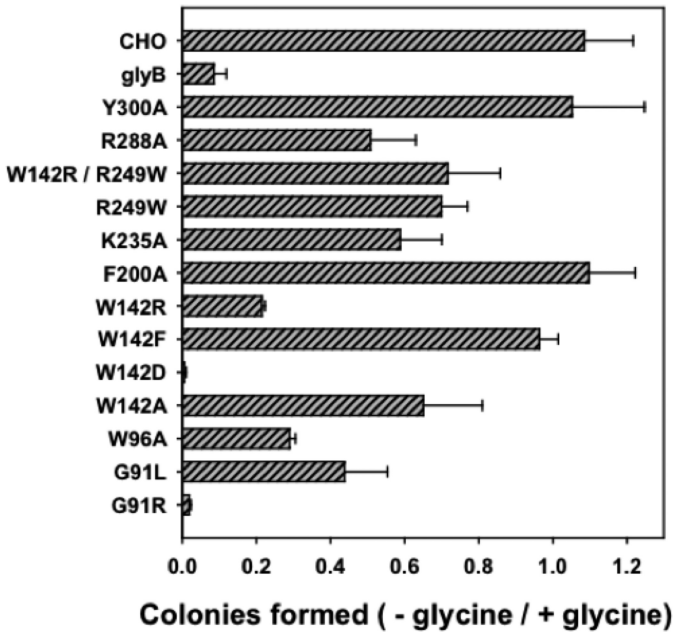

FIGURE 6. **glyB complementation of glycine auxotrophy with MFT mutant proteins.** glyB cells were plated at 1×10^5 cells/100-mm dish and transfected with a cDNA encoding the indicated MFT mutant protein to examine whether the expressed mutant MFT protein could facilitate sufficient mitochondrial folate transport to alleviate the glycine auxotrophy of glyB cells. Data are expressed as a ratio of colonies formed in medium with 1 mg/ml Geneticin without glycine *versus* colonies formed in medium with both Geneticin and glycine. glyB cells were transfected with MFT wild-type hamster (CHO) and glyB MFT cDNAs as a positive control and a negative control, respectively. *Error bars* indicate S.D.

cant role in directing THF down into the transport cavity (Trp-96, Phe-200, Lys-235, Arg-288, and Tyr-300), alanine-substituted mutants did not facilitate efficient mitochondrial folate uptake (Fig. 5*B*). Hence, we concluded that these several residues were involved in the recruitment of THF to the base of the MFT transport cavity.

glyB Complementation by MFT Mutant Proteins—We have previously shown that the glycine auxotrophy of glyB cells could be complemented by stable transfection with a cDNA encoding a functional MFT protein, and we have also used this system to test the function of mutated MFT species (2, 3, 13). Hence, when glyB cells were transfected with the wild-type hamster MFT cDNA (CHO), they survived equally well in the absence of glycine as in its presence, whereas glyB cells transfected with glyB MFT cDNA were unable to survive in the absence of glycine (Fig. 6). Survival in this complementation assay has previously been linked with a restoration of mitochondrial folate accumulation, measured over a period of days (2, 3). It appears that complementation, measured over a period of 10 days, rather than the 4 min used in the transport assay in Figs. 4 and 5, reflects the ability to transport folates albeit even at a slow rate equivalent to the replacement of the mitochondrial folate content once during a cell doubling time (16 h).[3] Only two mutations, W142D and G91R, were unable to complement glyB cells, suggesting that these mutant proteins were completely devoid of transport activity. These two mutations replaced the residues at codons 142 and 91 that are used in all of the nucleotide transporters of the MCF family. Clearly, these substitutions were absolutely required to allow the evolution of a transporter capable of translocation of folates.

DISCUSSION

Here, we studied the function of the MFT by site-specific mutagenesis of amino acid residues suggested by MD simulations to play a role either in the transit of THF down the transport cavity or in positioning of THF at the base of the cavity. Only one protein of the MCF has yielded to structural analysis by x-ray crystallography, the bovine AAC (7). However, the sequence homology between members of the family and the characteristics of the AAC structure appear to be conducive to the construction of very good quality homology models of other MCF members based on the use of the AAC structure as a scaffold. Thus, the bovine AAC structure is that of a 297-residue protein with 57% of its residues forming six transmembrane α-helical domains, three of which have a distinctive bend located two-thirds of the distance into an obvious aqueous cavity; the position of the bend is marked by the P*X*(D/E)*XX*(K/R) motif (7). All MCF members have the same size (290–350 residues) with six clearly predicted α-helical domains and with the odd-numbered helices segmented two-thirds along the helical domain by this conserved signature motif. A sequence comparison of the bovine AAC with the hamster MFT is shown in supplemental Fig. 1. Several studies of MCF members have used homology modeling and computational docking to visu-

[3] The clonogenicity of CHO cells was only reduced to 50% when mitochondrial folate pools were reduced to 3% of control. We concluded that the complementation assay reflects a much more dramatic decrease in MFT function than does the transport assay and that only the transport data directly reflected transport efficiency.

alize the general structure and putative substrate-binding pockets of these proteins, including our previous study on the MFT protein (9, 13, 35–37). In addition, several MD simulations have been published on the AAC protein, including studies in which the dynamics of entry of ADP into the aqueous cavity were examined (10, 38–40). Although these homology modeling and MD studies have been arguably very valuable to the field, they are not without limitations; they are both computational extensions of structural information that cannot easily be experimentally validated. In this study, we pushed these extrapolations further by combining what appears to be a high quality homology model with MD simulations of substrate entry into the MFT transport channel. However, we did so for the express purpose of making predictions of residues that would be informative in site-directed mutagenesis experiments. We found that the MD simulations with the MFT identified residues that were required for folate transport with remarkable accuracy; every residue suggested to guide the THF down into the channel or fix its position at the base of this cavity proved important to MFT function by mutagenesis. This approach has yielded the highest frequency of such informative mutations that we have experienced to date. This experimental verification of predictions made from MD simulations lends a degree of validity to the insights gained from our *in silico* studies.

A clear advantage of MD simulations was that they allowed a visualization of substrate capture by the MFT. These *in silico* studies predicted that MFT residues located high up in the transport channel guided a path of folate descent that was regimented well before the bottom of the transport cavity. The trajectory of the folate substrate was dictated by several sets of sequential interactions, each set being prerequisite for the next. Channel-lining residues simultaneously coordinated the pteridine, the phenyl, and the carboxylate groups of the THF molecule within the transport cavity at each discrete step during descent. For descent to occur, one group on the THF molecule transiently released from a residue to which it was loosely bound, while the other interactions between THF and channel residues remained intact. Following each momentary release, the substrate needed to be properly positioned and have the flexibility to make contact with another complementary residue located deeper within the transport cavity in a series of ratchet-like motions. After establishing contact with a residue located deeper within the MFT transport cavity, the substrate would then break away from the interaction set higher in the channel and form a new interaction set deeper within the transport cavity. In this manner, substrate descent was highly coordinated, and the chemical and spatial characteristics of the substrate molecule were tested at every level of descent with every new set of interactions. The flexibility of the substrate coupled with the spacing of complimentary bonding groups on the substrate and residue side chains are likely the most important factors in substrate recognition and efficient transport.

We conducted several MD simulations that were reproducible and remarkably consistent with previous MD studies on the solved AAC crystal structure. A total of three MD simulations all faithfully reproduced the trajectory shown in Fig. 1, and the same set of interactions occurred in each simulation, irrespective of the starting orientation of THF (supplemental Fig. 3). Interestingly, when a THF molecule was introduced into the transport cavity with the pteridine ring of THF facing down, the THF did not engage with residues farther into the cavity until the THF molecule reoriented into a position with the carboxylate groups pointing down, in a dive-like motion (supplemental Fig. 4). The reorientation effect of tetrahydrofolate was quite striking and was similar to what was demonstrated in MD simulations of an ADP molecule in the AAC transport cavity (39, 40). The reorientation of the ADP substrate was previously attributed the positive electrostatic potential calculated at the base of the AAC transport cavity (39, 40). We noted that the MFT also contained a large positive electrostatic potential at the base of the transport cavity. This positive electrostatic potential appears to be the force orienting the THF substrate so that it descends into the transport cavity with the negatively charged carboxylates down.

Our MD simulations identified three residues located at the base of the MFT transport cavity (Gly-91, Trp-142, and Arg-249) that held THF in position for an extended period of time. Although almost all MCF transporters carry a (D/E) at MFT 142, we found that the MFT absolutely cannot function with a (D/E) residue at this position. In addition to the Trp substitution definitive of this subfamily, all P(I/L)W transporters contain a Gly at MFT 91, whereas the closely related MCF nucleotide transporters and several other MCF proteins require a Lys or an Arg at this position for function (11, 33, 34). Gly-91 was predicted to be very close to Trp-142 at the base of the cavity. We also demonstrated that the MFT absolutely could not function with an Arg at position 91. Several other mutations at MFT positions 91, 142, and 249 impaired the ability of the MFT to facilitate folate uptake; the protein was quite intolerant of mutations at these sites. In fact, the only mutations that permitted efficient mitochondrial folate uptake in transport assays were two constructs (W142F and W142R/R249W) that allowed formation of the proposed π-cation interaction. Although these data reinforce the concept of a role for a π-cation bond between these residues in mitochondrial folate transport, we noted that MFT Trp-142 was also predicted in our MD simulations to position the THF substrate at the base of the transport cavity, suggesting multiple roles for this residue in the overall folate transport mechanism. Nonetheless, it is now clear from these studies that this tryptophan substitution is central to the transport mechanism of the MFT and likely all P(I/L)W family members.

Alanine-scanning mutagenesis of MFT residues Trp-96, Phe-200, Lys-235, Arg-288, and Tyr-300, which were predicted to be located higher up in the transport cavity and to interact with the substrate during descent, demonstrated that these residues were required for efficient MFT function. These residues highlight similarities and differences between the MFT and other MCF proteins. Sequence homology shows that almost every MCF member contains a Lys or an Arg at the position equivalent to MFT Arg-288 (9). This (K/R) residue is required for transport in every MCF protein in which it has been mutated (11, 33, 34); we also showed MFT Arg-288 to be required for folate transport (Fig. 5*B*). Likewise, most MCF members contain a tyrosine residue, or at least an aromatic side chain residue, at the position equivalent to MFT Tyr-300. Con-

sistent with our data, Cappello *et al.* (34) showed that mutation of the homologous position (Phe-299) impaired the function of the oxoglutarate transporter. Thus, it seems likely that MFT Arg-288 and Tyr-300, although needed for efficient folate transport, serve a function common to all MCF transporters and are not closely linked to substrate specificity.

MFT Phe-200 was required for optimal folate transport and was predicted to contact THF during descent into the cavity. The residues at this position in bovine transporters, the oxoglutarate transporter (Gln-198) and AAC (Phe-191), are also required for function (41, 42), suggesting that this position may be involved in general substrate discrimination between keto acid (the oxoglutarate transporter) and nucleotide/nucleotide-like (AAC and MFT) substrates. Although the AAC and MFT are both considered to be members of the nucleotide transporter subfamily, it is worthwhile to note that AAC Phe-191 is located in an aromatic ladder structure on TMD 4 that is thought to coordinate the adenine ring of ADP (7, 39, 40), whereas our MD simulations predict the pteridine ring of THF to predominantly contact an aromatic residue (Trp-96) on MFT TMD 2 instead. Hence, despite the MFT and AAC displaying the same residue at this position, MFT Phe-200 may play a different role in folate transport than in ADP transport.

Finally, our studies identified residues required for MFT function that were conserved in P(I/L)W proteins but were not present in the vast majority of other MCF transporters. All P(I/L)W transporters contain a Lys at the position equivalent to MFT 235, whereas only one other MCF member out of the 40 analyzed by Robinson and Kunji (9) contains a lysine at this position, suggesting that this residue may be involved in the discrimination of P(I/L)W substrates from all other MCF substrates. Furthermore, no non-P(I/L)W MCF protein contains a tryptophan at MFT 96, and more interestingly, neither does the yeast P(I/L)W subfamily member, Rim2p, a pyrimidine transporter (43). It is possible that this sequence difference may confer the substrate specificity for the Rim2p protein among the P(I/L)W subfamily.

Although we discovered residues important for MFT function that were different from other non-P(I/L)W MCF members and even one P(I/L)W subfamily protein, Rim2p, the residues that distinguish the MFT from the remaining P(I/L)W proteins, yeast Flx1p (FAD^+) (44) and yeast Ndt1p (NAD^+) (45), were not evident. This begs the question of how P(I/L)W transporters of folate, FAD^+, and NAD^+ discriminate between their substrates among themselves. Interestingly, reconstitution studies that defined the yeast Ndt1p protein as the mitochondrial transporter of NAD^+ showed that this protein could also transport FAD^+ to a lesser extent (45). Furthermore, it was previously shown that transfection of human MFT cDNA into a Flx1p-mutated yeast strain restored growth of this strain, suggesting that the MFT may be capable of facilitating FAD^+ transport (46). However, we did not observe any glyB complementation when glyB cells were transfected with cDNAs encoding the yeast Flx1p or Ndt1p proteins (3). Nonetheless, the possibility that there may be crossover of transport function between these closely related proteins warrants clarification by substrate specificity studies in reconstituted systems. It is interesting that the MFT is the only mammalian P(I/L)W protein of the five identified transporters. It is possible that mitochondrial transport of FAD^+, NAD^+, and folates, and maybe even pyrimidines, is all performed by the MFT in mammalian systems.

Acknowledgment—We are grateful to the Ohio Supercomputer Center for a generous allocation of computational resources.

REFERENCES

1. Kao, F., Chasin, L., and Puck, T. T. (1969) *Proc. Natl. Acad. Sci. U.S.A.* **64,** 1284–1291
2. McCarthy, E. A., Titus, S. A., Taylor, S. M., Jackson-Cook, C., and Moran, R. G. (2004) *J. Biol. Chem.* **279,** 33829–33836
3. Titus, S. A., and Moran, R. G. (2000) *J. Biol. Chem.* **275,** 36811–36817
4. Freemantle, S. J., Taylor, S. M., Krystal, G., and Moran, R. G. (1995) *J. Biol. Chem.* **270,** 9579–9584
5. Lin, B. F., Huang, R. F., and Shane, B. (1993) *J. Biol. Chem.* **268,** 21674–21679
6. Palmieri, F. (2004) *Pflugers Arch.* **447,** 689–709
7. Pebay-Peyroula, E., Dahout-Gonzalez, C., Kahn, R., Trézéguet, V., Lauquin, G. J., and Brandolin, G. (2003) *Nature* **426,** 39–44
8. Nelson, D. R., Felix, C. M., and Swanson, J. M. (1998) *J. Mol. Biol.* **277,** 285–308
9. Robinson, A. J., and Kunji, E. R. (2006) *Proc. Natl. Acad. Sci. U.S.A.* **103,** 2617–2622
10. Falconi, M., Chillemi, G., Di Marino, D., D'Annessa, I., Morozzo della Rocca, B., Palmieri, L., and Desideri, A. (2006) *Proteins* **65,** 681–691
11. Ma, C., Remani, S., Sun, J., Kotaria, R., Mayor, J. A., Walters, D. E., and Kaplan, R. S. (2007) *J. Biol. Chem.* **282,** 17210–17220
12. Dougherty, D. A. (1996) *Science* **271,** 163–168
13. Perchiniak, E., Lawrence, S. A., Kasten, S., Woodard, B. A., Taylor, S. M., and Moran, R. G. (2007) *Biochemistry* **46,** 1557–1567
14. Bryson, K., McGuffin, L. J., Marsden, R. L., Ward, J. J., Sodhi, J. S., and Jones, D. T. (2005) *Nucleic Acids Res.* **33,** W36–W38
15. Tripos International (2008) *Sybyl 8.0 ORCHESTRAR*, Tripos International, St. Louis, MO
16. Humphrey, W., Dalke, A., and Schulten, K. (1996) *J. Mol. Graph.* **14,** 33–38
17. Phillips, J. C., Braun, R., Wang, W., Gumbart, J., Tajkhorshid, E., Villa, E., Chipot, C., Skeel, R. D., Kalé, L., and Schulten, K. (2005) *J. Comput. Chem.* **26,** 1781–1802
18. MacKerell, A. D., Bashford, D., Bellott, Dunbrack, R. L., Evanseck, J. D., Field, M. J., Fischer, S., Gao, J., Guo, H., Ha, S., Joseph-McCarthy, D., Kuchnir, L., Kuczera, K., Lau, F. T. K., Mattos, C., Michnick, S., Ngo, T., Nguyen, D. T., Prodhom, B., Reiher, W. E., Roux, B., Schlenkrich, M., Smith, J. C., Stote, R., Straub, J., Watanabe, M., Wiorkiewicz-Kuczera, J., Yin, D., and Karplus, M. (1998) *J. Phys. Chem. B* **102,** 3586–3616
19. Dolinsky, T. J., Czodrowski, P., Li, H., Nielsen, J. E., Jensen, J. H., Klebe, G., and Baker, N. A. (2007) *Nucleic Acids Res.* **35,** W522–W525
20. Bas, D. C., Rogers, D. M., and Jensen, J. H. (2008) *Proteins* **73,** 765–783
21. Kieseritzky, G., and Knapp, E. W. (2008) *Proteins* **71,** 1335–1348
22. Feller, S. E., Zhang, Y., Pastor, R. W., and Brooks, B. R. (1995) *J. Chem. Phys.* **103,** 4613–4621
23. Martyna, G. J., Tobias, D. J., and Klein, M. L. (1994) *J. Chem. Phys.* **101,** 4177–4189
24. Garcia-Viloca, M., Truhlar, D. G., and Gao, J. (2003) *Biochemistry* **42,** 13558–13575
25. Breneman, C. M., and Wiberg, K. B. (1990) *J. Comput. Chem.* **11,** 361–373
26. Becke, A. D. (1988) *Phys. Rev. A* **38,** 3098–3100
27. Becke, A. D. (1993) *J. Chem. Phys.* **98,** 1372–1377
28. Lee, C., Yang, W., and Parr, R. G. (1988) *Phys. Rev. B* **37,** 785–789
29. Frisch, M. J., Trucks, G. W., Schlegel, H. B., Scuseria, G. E., Robb, M. A., Cheeseman, J. R., Montgomery, J., J. A., Vreven, T., Kudin, K. N., Burant, J. C., Millam, J. M., Iyengar, S. S., Tomasi, J., Barone, V., Mennucci, B., Cossi, M., Scalmani, G., Rega, N., Petersson, G. A., Nakatsuji, H., Hada, M., Ehara, M., Toyota, K., Fukuda, R., Hasegawa, J., Ishida, M., Nakajima, T.,

Honda, Y., Kitao, O., Nakai, H., Klene, M., Li, X., Knox, J. E., Hratchian, H. P., Cross, J. B., Bakken, V., Adamo, C., Jaramillo, J., Gomperts, R., Stratmann, R. E., Yazyev, O., Austin, A. J., Cammi, R., Pomelli, C., Ochterski, J. W., Ayala, P. Y., Morokuma, K., Voth, G. A., Salvador, P., Dannenberg, J. J., Zakrzewski, V. G., Dapprich, S., Daniels, A. D., Strain, M. C., Farkas, O., Malick, D. K., Rabuck, A. D., Raghavachari, K., Foresman, J. B., Ortiz, J. V., Cui, Q., Baboul, A. G., Clifford, S., Cioslowski, J., Stefanov, B. B., Liu, G., Liashenko, A., Piskorz, P., Komaromi, I., Martin, R. L., Fox, D. J., Keith, T., Al-Laham, M. A., Peng, C. Y., Nanayakkara, A., Challacombe, M., Gill, P. M. W., Johnson, B., Chen, W., Wong, M. W., Gonzalez, C., and Pople, J. A. (2004) *Gaussian 03*, Gaussian, Inc., Wallingford CT

30. Sanbrook, J., and Russel, D. W. (2001) *Molecular Cloning: A Laboratory Manual*, 3rd Ed., Cold Spring Harbor Press, Cold Spring Harbor, NY
31. Graham, F. L., and van der Eb, A. J. (1973) *Virology* **52,** 456–467
32. Aksimentiev, A., and Schulten, K. (2005) *Biophys. J.* **88,** 3745–3761
33. Nelson, D. R., Lawson, J. E., Klingenberg, M., and Douglas, M. G. (1993) *J. Mol. Biol.* **230,** 1159–1170
34. Cappello, A. R., Curcio, R., Valeria Miniero, D., Stipani, I., Robinson, A. J., Kunji, E. R., and Palmieri, F. (2006) *J. Mol. Biol.* **363,** 51–62
35. Tonazzi, A., Giangregorio, N., Palmieri, F., and Indiveri, C. (2005) *Biochim. Biophys. Acta* **1718,** 53–60
36. Walters, D. E., and Kaplan, R. S. (2004) *Biophys. J.* **87,** 907–911
37. Morozzo Della Rocca, B., Miniero, D. V., Tasco, G., Dolce, V., Falconi, M., Ludovico, A., Cappello, A. R., Sanchez, P., Stipani, I., Casadio, R., Desideri, A., and Palmieri, F. (2005) *Mol. Membr. Biol.* **22,** 443–452
38. Johnston, J. M., Khalid, S., and Sansom, M. S. (2008) *Mol. Membr. Biol.* **25,** 506–517
39. Dehez, F., Pebay-Peyroula, E., and Chipot, C. (2008) *J. Am. Chem. Soc.* **130,** 12725–12733
40. Wang, Y., and Tajkhorshid, E. (2008) *Proc. Natl. Acad. Sci. U.S.A.* **105,** 9598–9603
41. David, C., Arnou, B., Sanchez, J. F., Pelosi, L., Brandolin, G., Lauquin, G. J., and Trézéguet, V. (2008) *Biochemistry* **47,** 13223–13231
42. Stipani, V., Cappello, A. R., Daddabbo, L., Natuzzi, D., Miniero, D. V., Stipani, I., and Palmieri, F. (2001) *Biochemistry* **40,** 15805–15810
43. Marobbio, C. M., Di Noia, M. A., and Palmieri, F. (2006) *Biochem. J.* **393,** 441–446
44. Tzagoloff, A., Jang, J., Glerum, D. M., and Wu, M. (1996) *J. Biol. Chem.* **271,** 7392–7397
45. Todisco, S., Agrimi, G., Castegna, A., and Palmieri, F. (2006) *J. Biol. Chem.* **281,** 1524–1531
46. Spaan, A. N., Ijlst, L., van Roermund, C. W., Wijburg, F. A., Wanders, R. J., and Waterham, H. R. (2005) *Mol. Genet. Metab.* **86,** 441–447